Early structural development in melt-quenched polymer PTT from atomistic molecular dynamic simulations

2009 J. Phys.: Condens. Matter 21 505101

(http://iopscience.iop.org/0953-8984/21/50/505101)

J. Phys.: Condens. Matter **21** (2009) 505101 (10pp) doi:10.1088/0953-8984/21/50/505101

Early structural development in melt-quenched polymer PTT from atomistic molecular dynamic simulations

Min-Kang Hsieh and Shiang-Tai Lin[1]

Department of Chemical Engineering, National Taiwan University No. 1, Section 4, Roosevelt Road, Taipei 10617, Taiwan

E-mail: stlin@ntu.edu.tw

Received 30 May 2009, in final form 18 August 2009
Published 13 November 2009
Online at stacks.iop.org/JPhysCM/21/505101

Abstract

Molecular dynamics simulations are performed to study the initial structural development in poly(trimethylene terephthalate) (PTT) when quenched below its melting point. The development of local ordering has been observed in our simulations. The thermal properties, such as the glass transition temperature (T_g) and the melting temperature (T_m), determined from our simulations are in reasonable agreement with experimental values. It is found that, between these two temperatures, the number of local structures quickly increases during the thermal relaxation period soon after the system is quenched and starts to fluctuate afterwards. The formation and development of local structures is found to be driven mainly by the torsional and van der Waals forces and follows the classical nucleation–growth mechanism. The variation of local structures' fraction with temperature exhibits a maximum between T_g and T_m, resembling the temperature dependence of the crystallization rate for most polymers. In addition, the backbone torsion distribution for segments within the local structures preferentially reorganizes to the trans–gauche–gauche–trans (t–g–g–t) conformation, the same as that in the crystalline state. As a consequence, we believe that such local structural ordering could be the baby nuclei that have been suggested to form in the early stage of polymer crystallization.

(Some figures in this article are in colour only in the electronic version)

1. Introduction

In the classical theory of nucleation, the crystallization of a material when cooled to a temperature below its melting point is generally recognized to be a two-stage process. In the stage of primary nucleation, crystal nuclei (clusters comprising ordered molecules) appear and redissolve via molecular collisions until the size of a nucleus reaches some critical value, above which the nuclei are thermodynamically stable. The subsequent growth of the critical nuclei follows a kinetic mechanism and is classified as a growth process. Complicated by additional constraints in topological connectivity, the crystallization in polymers presents remarkable differences both in the nucleation and in the growth stages when compared to that in small molecules. While extensive experimental [1–4] and theoretical [5–9] efforts are made to verify and explain the molecular mechanism in the growth of nuclei in polymeric materials, the primary stage of polymer crystallization [10–12] is less well understood. Experimental results from small-angle x-ray [13–15] and dielectric spectroscopy [16, 17] measurements suggest the development of large-scale structures prior to any detectable formation of crystallites. This has led some researchers to believe in the formation of a precursor phase via spinodal decomposition at the early stage of polymer crystallization. The existence of nucleus precursors may be attributed to the memory effects in polymeric materials [18]. However, with the enhancement of resolution in scattering measurements, such a view is continuously challenged by some researchers [19–23], who believe that the crystallization should follow the classical nucleation–growth mechanism.

[1] Author to whom any correspondence should be addressed.

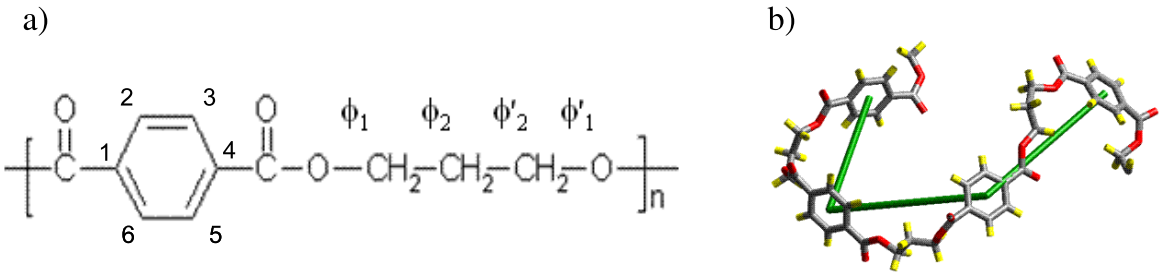

Figure 1. The chemical structure of a repeating unit of PTT (a) and a fragment (four repeating units) of the PTT chain (b). Carbon atoms are shown in gray, oxygen in dark gray (red online) and hydrogen in light gray (yellow online). The (green) cylinders connecting the centers of the adjacent aromatic rings are taken as elementary segments in the cluster analysis.

Molecular dynamics simulations provide a useful perspective from a molecular scale for studying the mechanism of polymer crystallization. Most simulation studies focus on the stress- (or flow-) induced crystallization phenomenon by pre-oriented chains [24–29] and extensional flow field [30], while a few of them investigate the crystallization driven by the sub-melting-point temperature [9, 31–36]. Recently Gee *et al* [32] used molecular dynamic simulation techniques to study the primary nucleation of poly(vinylidene fluoride), PVDF, and polyethylene, PE. They reported the formation of a precursor phase via spinodal decomposition as the polymer melt is quenched into the unstable state.

In this work, we use fully atomistic models to simulate the initial stage of the crystallization process of poly(trimethylene terephthalate), PTT. Unlike coarse-grained or bead–spring models that are more often adopted in the simulation for crystallization processes of polymers [32, 37–40], atomistic molecular models, while more computationally demanding, provide a much better resolution of the detailed packing structure. PTT [1–3, 41–54], a member of the aromatic polyesters, exhibits outstanding elastic recovery and resiliency properties over its homologous sisters PET and PBT [55]. PTT consists of a rigid terephthalic group and a flexible trimethylene group, and shows a zigzag chain conformation in the crystalline state. Our simulations reveal that highly ordered but loosely packed clusters are formed as soon as the liquid polymer is quenched below its melting point. The number of such clusters reaches a maximum between the melting and glass transition temperatures. The formation and development of these clusters follows the nucleation and growth mechanism. In addition, it is observed that the torsion distribution of the segments within the clusters preferentially organizes to that of the crystalline state. It is thus believed that these clusters behave like baby nuclei [5, 56] in polymer nucleation and may play an important role in polymer crystallization.

2. Computational methods

The early-stage crystallization process of PTT, whose chemical structure is shown in figure 1, is studied here. The initial structures of PTT are prepared using the Amorphous Builders module implemented in the commercial package Cerius2 [57]. Two different sized systems are used in this study. The smaller system contains four chains of PTT molecules, each having a degree of polymerization of 27 (i.e. 5568 g mol^{-1}. Note that the entanglement molecular weight of PTT was determined to be 4900–5000 g mol^{-1} [49, 58]) and the larger sized system contains eight chains of the same molecules. The small sized models (containing 108 repeating units of PTT, or equivalently 2708 atoms) are used in most studies whereas the larger systems are used for examining the system size effects. The computer code LAMMPS [59] is used for all subsequent molecular mechanics and molecular dynamics simulations. A series of expansion and compression steps were applied to the initial structures in order to obtain equilibrium samples at 600 K (which is above the melting temperature T_m). The equilibration process proceeded as follows. The simulation box is first expanded via increasing the cell lengths by 125% (e.g. from 30.53 to 33.58 Å for small systems) over a period of 60 ps. The box is then compressed by reducing the cell lengths to 95% of the initial values (from 33.58 to 29 Å) over a period of 100 ps. The cell lengths are then increased to their initial values within 50 ps (from 29 to 30.53 Å). Finally, the simulation box is equilibrated at 600 K using the NPT ensemble for 100 ps. The equilibrated sample is then cooled to 50 K at a rate of 1 K ps^{-1}. At each 50 K interval during the quenching process, simulation samples are taken and subjected to long (up to 24 ns), constant temperature and pressure simulations (NPT) for property analysis. Long-range interactions are included using the particle-mesh Ewald method [60, 61] and the Nose–Hoover thermostat [62, 63] with a time constant of 0.01 ps used to control the temperature. The integration time step used is 0.5–1 fs. The simulations presented in this work amount to 5×10^4 CPU hours on one Intel Xeon 3.0 GHz processor.

In all the simulations, the generic force field, Dreiding [64], is used to describe the valence (bond stretching, angle bending, torsion angle rotation and inversion) and van der Waals interactions among the atoms in a system. A generic force field, Dreiding, is chosen here because its parameters were not optimized against any specific properties of any specific systems. Such a type of force field is not biased (in terms of accuracy) towards any property of a system and is considered more suitable for studying physical phenomena not considered in the parameterization. All the default values were used except for the torsion terms of the propylene glycol segment (O–CH$_2$–CH$_2$–CH$_2$–O) being modified to better reproduce QM results. (The parameters for 'C_R O_R C_3 X'

Table 1. Comparison of the lattice parameters, density and torsional angles of crystalline PTT.

	Expt1 [70]	Expt2 [71]	Simulation [42]	MD[a]
a (Å)	4.637	4.59	4.50 ± 0.14	4.40 ± 0.05
b (Å)	6.266	6.21	6.05 ± 0.18	6.33 ± 0.06
c (Å)	18.46	18.31	18.83 ± 0.44	18.84 ± 0.15
α (deg)	98.4	98.0	98.00 ± 1.28	101.7 ± 0.7
β (deg)	93.0	90.0	91.18 ± 1.99	90.0 ± 0.4
γ (deg)	111.1	111.7	111.50 ± 0.57	110.2 ± 1.1
ρ (g cm^{-3})	1.387	1.43	—	1.42 ± 0.02
ϕ_1 (deg)	($\pm$175)	167.4	—	175.0 ± 4.4
ϕ_2 (deg)	($\pm$60)	−73.7	—	-64.8 ± 8.6
ϕ_2' (deg)	—	−61.9	—	-64.7 ± 8.6
ϕ_1' (deg)	—	−152.8	—	-162.7 ± 10.3

[a] Results averaged from MD simulations performed on a PTT crystalline unit cell at 0 bar and 300 K for 300 ps.

Table 2. Comparison of the thermal properties (T_g and T_m) and mechanical property (Young's modulus) of amorphous PTT.

	Expt	MD simulation[a]
Glass transition temperature (T_g) (K)	315–348 [3, 41]	360 ± 15
Melting temperature (T_m) (K)	499–503 [1, 3, 50]	$\sim 550 \pm 25$
Young's modulus (GPa)	2.3 ∼ 2.8 [41, 55, 72]	2.72 ± 0.54

[a] MD results from simulations performed on amorphous PTT (simulation parameters are detailed in the text).

torsion in Dreiding $E_{\text{torsion}}(\phi) = \sum_{n=1}^{p} \frac{1}{2} K_n[1 - d\cos(n\phi)]$ were modified from $n = 6, d = 1, K_6 = 1$ kcal mol^{-1} to $n = 3, d = -1, K_3 = 2$ kcal mol^{-1}.) Atomic (Mulliken) charges, for describing Coulomb interactions, are determined from density functional theory (DFT) calculations for the monomer of PTT using the B3LYP functional [65–67] and 6-31G** basis set [68] in Gaussian 98 [69].

3. Results and discussion

3.1. Force field validation

Table 1 compares the lattice parameters, torsional angles (ϕ_1, ϕ_2, ϕ_1' and ϕ_2' as indicated in figure 1) and density of crystalline PTT from simulation and experiment [70, 71]. In general, the simulation results are in good agreement with experiment. It is interesting to note that the asymmetric torsional angles ($\phi_1 \neq \phi_1'$ and $\phi_2 \neq \phi_2'$) observed in experiment are also seen in our simulation.

Table 2 lists the mechanical and thermal properties of PTT. The calculated elastic constant, determined from the slope of the stress and strain curve, is 2.72 ± 0.54 GPa, in good agreement with the experimental measurement of 2.3–2.8 GPa [41, 55, 72] and other simulation results 3.84 ± 0.16 GPa [49]. (The elastic constant is determined from the average of stress–strain curves from constant rate expansion–compression simulations in the x, y, z directions, respectively, at 300 K. Several deformation rates were studied, from 1×10^9 to 1×10^{11} s^{-1}. The simulation details can be found elsewhere [73].) The melting temperature (T_m) and glass transition temperature (T_g) are determined by examining the variation of density upon stepwise cooling and heating [74] at an effective rate of 1 K/1 ps, as shown in figure 2. Hysteresis in the density change is observed upon heating and cooling of an amorphous sample between 50 and 600 K. There is a change of slope at 350 K upon cooling and at 375 K upon heating. These results suggest that the T_g is about 360 ± 15 K (experimental value is 315–348 K [3, 41]). A semi-crystalline sample with an initial crystallinity of 18% is prepared and heated from 300 to 800 K. (The detailed procedure of the preparation and simulation of the semi-crystalline sample can be found elsewhere [73].) The density of the semi-crystalline sample decreases linearly with increasing temperature up to 550 K. Between 550 and 750 K, the density change becomes nonlinear. Beyond 750 K, density variation becomes linear again with a slope coinciding with that of the amorphous PTT. These results show that the crystalline region of the semi-crystalline sample starts to melt at 550 K (T_m, the experimental value is 499–503 K [1, 3, 50]). Therefore, the Dreiding force field can adequately describe many physical properties of PTT.

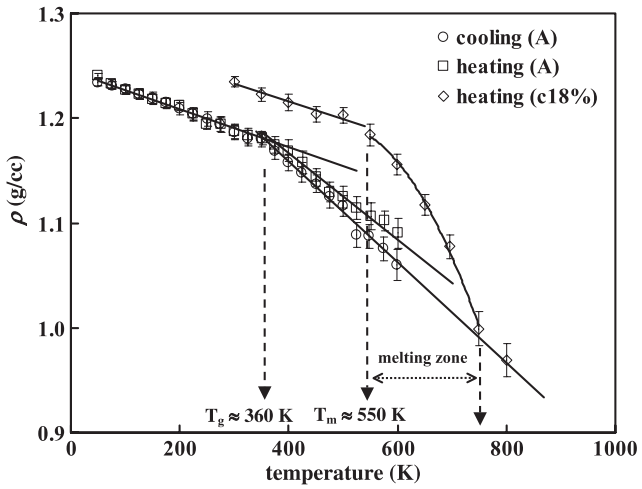

Figure 2. The density variation of PTT upon cooling and heating. A 600 K equilibrated amorphous sample (open circles) is cooled to 50 K and the 50 K equilibrated amorphous sample (open squares) is heated to a molten state. A semi-crystalline (18%) sample (open diamonds) is heated from 300 to 800 K. Each process was performed by step changes of temperature at an effective rate of 1 K ps^{-1}.

3.2. Energy and density

The time evolution of density and energy for PTT samples quenched to different temperatures is presented in figure 3. It can be seen that, for temperatures above 350 K (T_g), the densities (figure 3(a)) continue to rise and the potential energy (figure 3(b)) continues to decrease with time; while below 350 K, both properties remain constant, indicating the loss of mobility of the polymer chains. It is found that the variation in energy is dominated by the torsional angle rotation energy (figure 3(c)) and the van der Waals interaction (figure 3(d)), indicating that backbone rearrangement and chain packing are

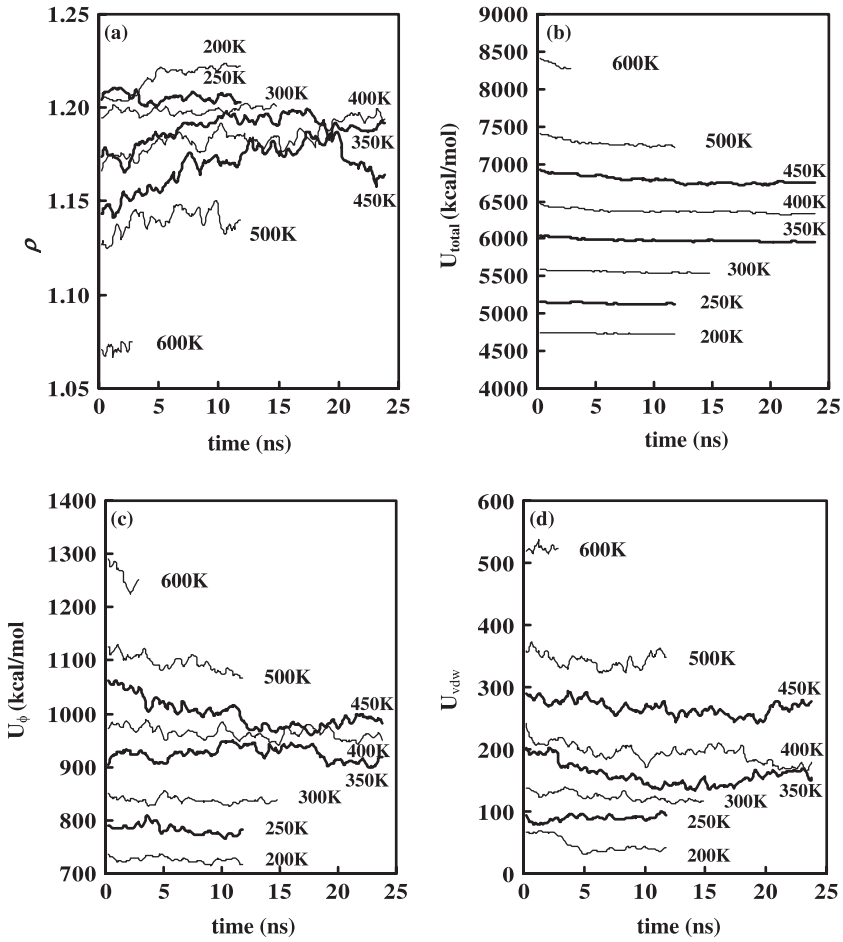

Figure 3. The time variation of density (a), total potential energy (b), torsion energy (c) and van der Waals energy (d) of PTT quenched from 600 K.

taking place. It is also interesting to note that the change in torsional angle rotation energy with time is different at 350, 400 and 450 K. (Note that longer (24 ns) simulations were performed for these three cases as they fall between T_g and T_m where nucleation processes may take place.) These results indicate that the mechanism of the torsional angle rotation in the crystallization could be different at various temperatures.

The increase of density for PTT at temperatures above 350 K is quite prominent. The variation in density shows a rapid increase at short time (<5 ns) and then progresses at a slower rate. The rapid density rise in a short time is a result of thermal relaxation after cooling, and the subsequent variation may indicate the progression of the phase transition for a long time. It should be noted that the simulated density of PTT melt at 600 K is 1.06 g cm^{-3} and the crystalline phase is 1.441 g cm^{-3}. The density values seen here indicate that the systems are still largely in an amorphous state.

3.3. Structure development in bulk PTT upon quenching

To detect and quantify any structural development, we define the local ordering in the system as follows. (1) A segment of PTT is defined to be the vector pointing from the center of an aromatic ring to the next aromatic ring on the same polymer chain (green cylinders in figure 1). (2) Adjacent segments are defined as those whose separation distance between centers of mass falls within 9 Å. (3) Two adjacent segments whose included angles are within 10° are marked as mutually parallel. (4) A locally ordered structure is identified as a cluster containing mutually parallel segments. The cluster defined by such criteria has an orientationally ordered but loosely packed structure. Based on this definition, we may easily determine the number n_s of clusters containing s parallel segments at any instant of time in the course of dynamic simulation. For example, the clusters identified from the NPT simulation at 400 K and six time instants are illustrated in figure 4. One can easily visualize the formation and development of such internally ordered clusters.

The local ordering within the system during the induction period of the crystallization process can be quantified by the 'fraction' of the aforementioned clusters. (Note that we have separately confirmed that the system as a whole remains isotropic at all temperatures, i.e. there is no long-ranged directional preference for the orientation of the clusters as one would expect from quenching.) First, we define the fraction X_s from clusters of size s as

$$X_s = s\langle n_s\rangle \Big/ \left(\sum_{i=1}^{\infty} i\langle n_i\rangle\right) \tag{1}$$

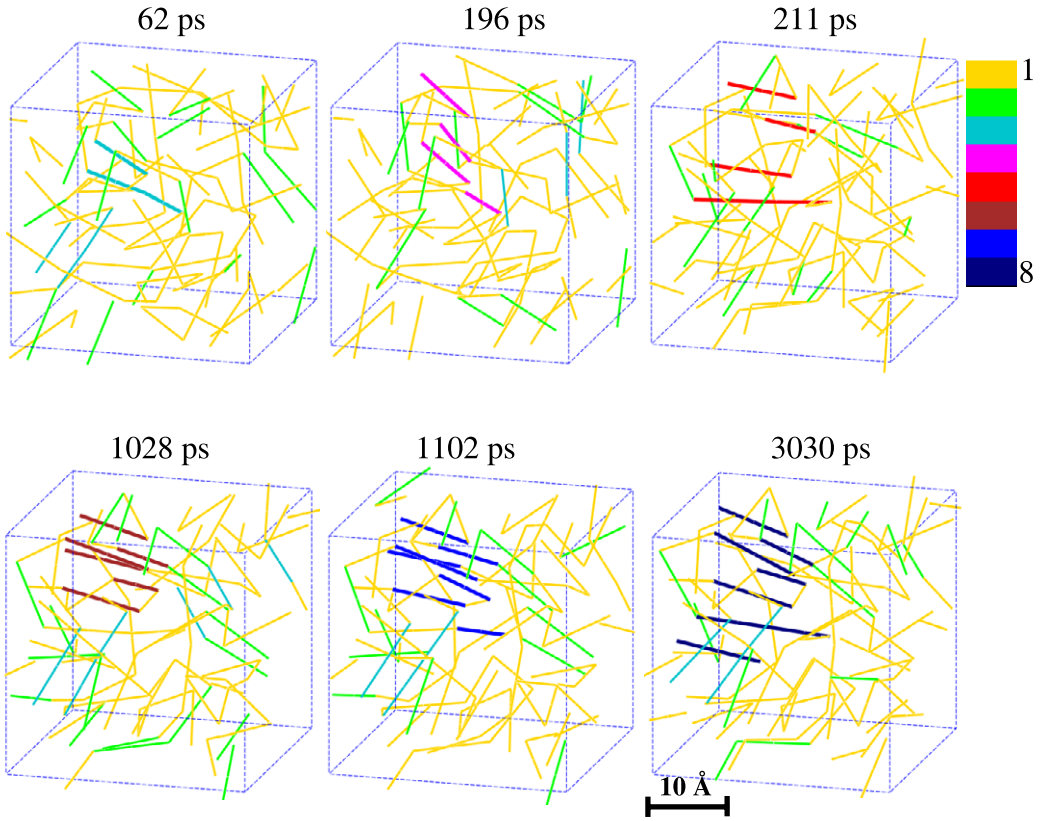

Figure 4. Illustration of the growth of orientationally ordered clusters from the melted state at 400 K. A color scale is used for better discrimination of the size of clusters.

where $\langle n_i \rangle$ is the average number of clusters of size i (i.e. the average value of n_i (calculated at every picosecond) over one nanosecond). (Note that $\sum_{i=1}^{\infty} i \langle n_i \rangle = 108$ is the number of repeating units in our simulation for small-sized systems.) The total fraction of clusters X is defined as

$$X = \sum_{s=4}^{\infty} X_s. \tag{2}$$

We have excluded the contributions from $s \leqslant 3$ because formation of such clusters highly depends on segment collisions and the value of the average number $\langle n_s \rangle$ is almost time-invariant at a given temperature. From figure 5, one can observe a clear trend of rapid enhancement of the fraction of local ordering, especially near 400 K, at the beginning of thermal equilibration. Afterwards, the amount of local ordering starts to fluctuate. Figure 5 also shows the average number of clusters as a function of temperature. Strikingly the temperature dependence of the fraction of clusters' curve resembles that of the crystallization rate for common polymers, i.e. having a maximum between T_g and T_m [75].

With a closer analysis of the simulation trajectory, we found that the formation and growth of these clusters is a highly dynamical process. In the liquid state (600 K) there is constant formation and disintegration of small clusters ($s = 2$, 3, 4 and 5) via segment vibration and collisions, i.e. these clusters are short-lived. As the system is quenched below T_m, some segments may agglomerate or deposit on a nearby cluster to form larger-sized clusters. In the subsequent NPT runs, these cluster may grow, break down to small clusters or dissolve back to the amorphous phase. Both the growth and disintegration of clusters are observed in this stage: however, the net effect

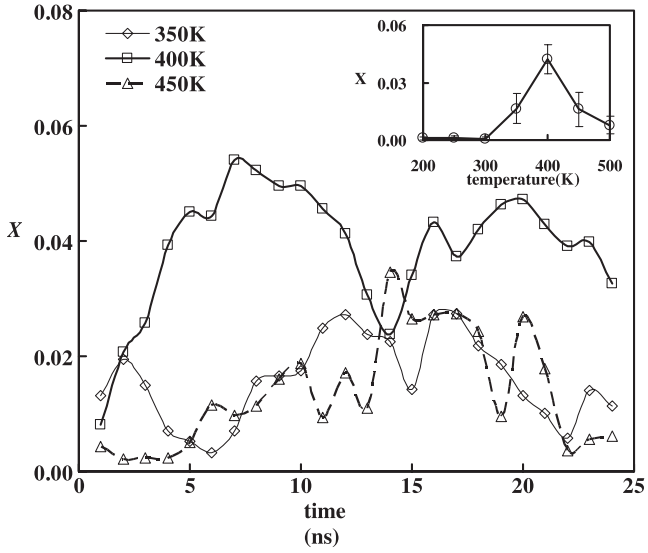

Figure 5. The variation of the number of clusters (defined in equation (2)) with time at 350 K, 400 K and 450 K. The inset shows the variation of the average number of clusters (defined in equation (2)) with temperature.

Table 3. The number and size of individual clusters identified in MD simulations.

Temperature (K)	Number of clusters[a]	Simulation length (ns)
Small size (108 segments)		
300	3 (5, 5, 5)	15
350	3 (9, 6, 5)	24
400	2 (9, 6)	24
450	3 (7, 7, 6)	24
Large size (216 segments)		
350	1(5)	12
400	9(7, 6, 6, 5, 5, 5, 5, 5, 5)	12
450	8(6, 5, 5, 5, 5, 5, 5, 5)	12

[a] Shown in parentheses is the maximum size s observed for each cluster.

(for a certain sized cluster to grow or dissolve) depends on the temperature and the size of the cluster (as it should be driven by thermodynamic equilibrium). As the temperature falls below T_g, small clusters become long-lived: however, most of them lose sufficient mobility to overcome barriers which prevent the formation and growth of larger clusters. As a consequence, we observe the presence of local ordering peaks at a temperature between T_g and T_m.

The observed mechanism of the formation and development of internally ordered clusters can also be explained using classical nucleation–growth theory, where the rate of crystallization is determined by the competition between the barriers to diffusion and nucleation. At high temperatures (close to T_m), segments have a higher mobility to overcome the diffusion barrier but there is little driving force to nucleation. At low temperatures, segments have a larger driving force to overcome the nucleation barrier but they have less mobility to overcome the diffusion barrier. Therefore, the evolution of such clusters seems to follow the nucleation–growth mechanism and may play a role in the nucleation and crystallization processes.

3.4. Structural development within orientationally ordered clusters

The structural development within the orientationally ordered clusters as a result of the interplay between the van der Waals and torsional forces can be better understood by analyzing its size (the number of segments), compactness (radial distribution function (RDF) from the representative atoms) and segment conformation (torsional angle distributions) of each individual cluster identified from section 3.3.

The number of clusters identified and some of their basic properties at temperatures from 300 to 450 K are summarized in table 3. In general, 2–3 clusters can be found in each sample (containing 108 segments). The time evolution of the size (the number of parallel segments contained in a cluster) of one representative cluster at different temperatures is shown in figures 7(a), (c) and (e). While the size of the cluster fluctuates, it can be seen that the cluster continues to grow throughout the duration of our simulation.

The RDF calculated from the 1, 4 carbon atoms on the aromatic ring (see figure 1) is used to quantify the segment

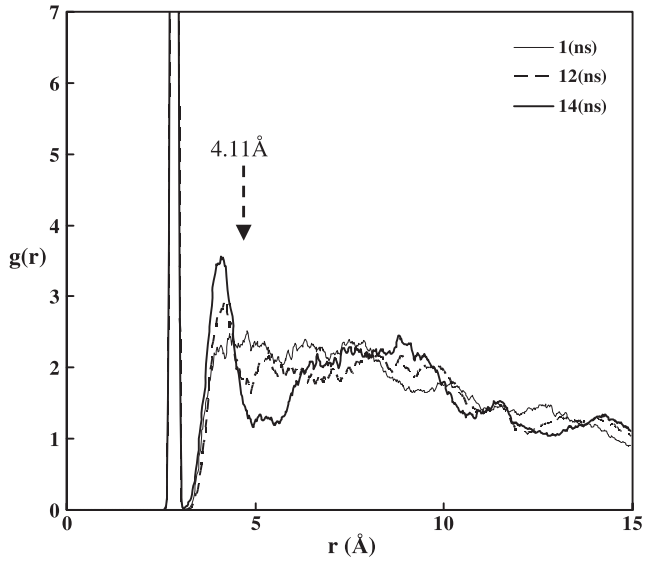

Figure 6. The radial distribution function calculated from the 1, 4 carbon atoms on the aromatic ring from a selected cluster whose largest size (at some time instant) is 9 ($s = 0$) in a system at 400 K.

packing within the cluster. Figure 6 illustrates such an RDF for a representative cluster at 400 K at different times. The first peak (2.85 Å) indicates the distance of the 1, 4 carbons on the same ring. The second peak (∼4.11 Å) is the characteristic to the parallel packing of aromatic rings (we have confirmed this via a separate simulation using crystalline PTT). It can be seen that the intensity of the second peak increases with time as a result of the better packing within the cluster. In figures 7(a), (c) and (e) the time variation of the intensity of this peak is shown for the largest clusters at 350, 400 and 450 K. (We have analyzed the properties for all clusters [73] and found that these cases are good representatives to explain the structural development within the clusters.) Although fluctuating, there is a general trend of enhancement of the peak intensity with time. The size (number of parallel segments) evolutions of the same clusters are shown on the same plots for comparison. It can be seen that, while both properties increase with time, there is no direct correlation between them. The result indicates that better packing of the segments could sometimes be compromised as the cluster grows in size, and vice versa.

Also shown in figures 7(b), (d) and (f) are time variations of the fractions of backbone torsions ϕ_1, ϕ_1' in the trans state and ϕ_2, ϕ_2' in the gauche state. (Note that we consider a torsion to be in the trans state if its angle ranges between (165°–180° and −165° to −180°) and in the gauche state between (45°–75° and −45° to −75°). Figure 8 shows the percentage of these torsions in the trans and gauche states. For segments within the clusters, the majority of $\langle\phi_1\rangle$ is in the trans state; however, there is no clear preferred state for the more flexible $\langle\phi_2\rangle$, although at high temperatures the gauche state appears to slightly dominate. The value of $\langle\phi\rangle$ is the time average of ϕ and ϕ' over a period of 1 ns. It can be seen that, for segments outside the orientationally ordered clusters (open symbols), the backbone torsions seem to be time-invariant. In contrast, within the clusters (closed symbols), the backbone

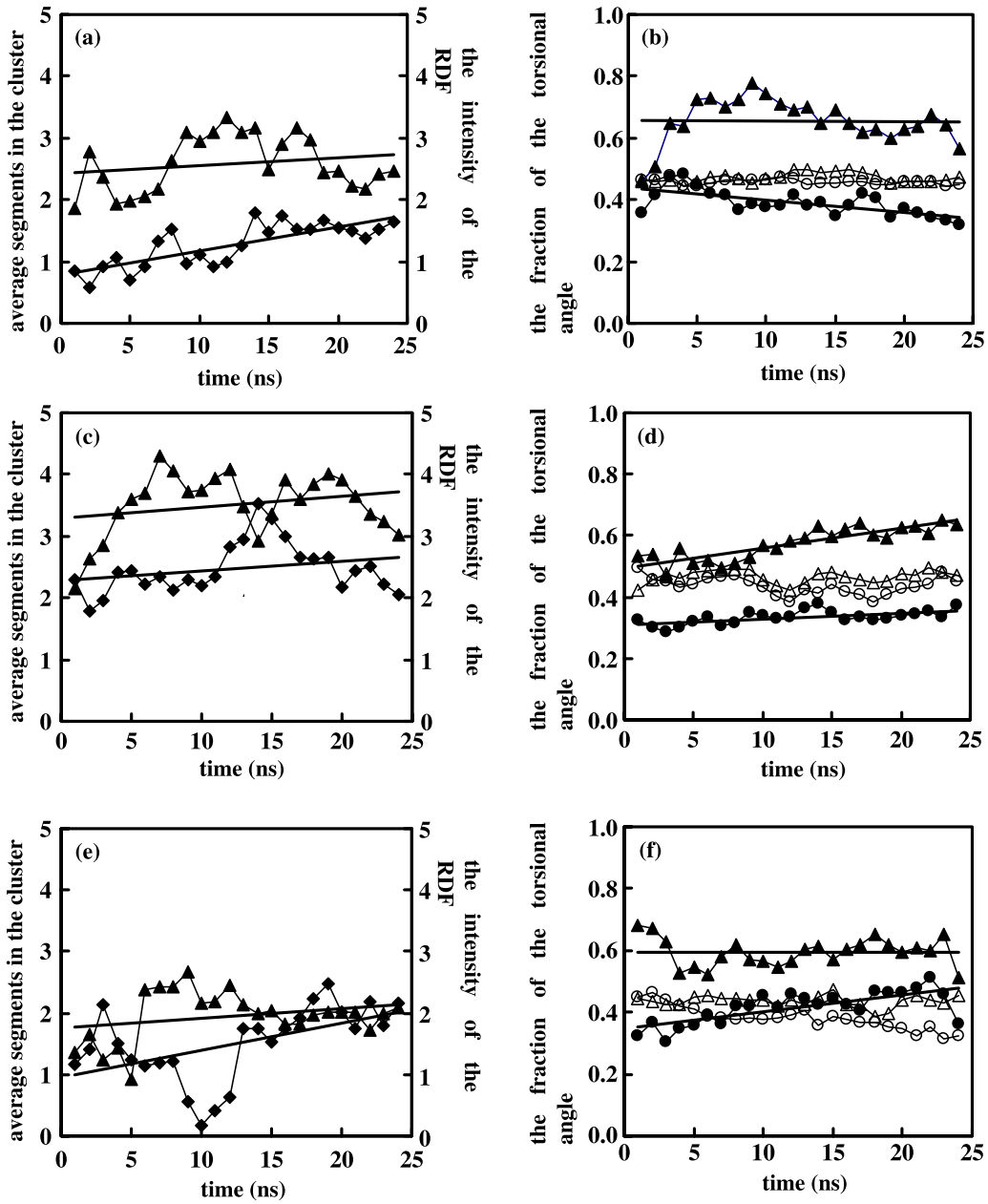

Figure 7. The time evolution of RDF intensity (4.11 Å) (in diamonds) and the time-averaged number of parallel segments contained in a representative cluster (in triangles) at 350 K (a), 400 K (c) and 450 K (e), and the backbone torsions $\langle\phi_1\rangle$ in trans (triangles) and $\langle\phi_2\rangle$ in gauche (circles) for segments in a cluster (closed symbols) and outside any cluster (open symbols) at 350 K (b), 400 K (d) and 450 K (f). The solid lines are the trend lines of the corresponding simulations for better visualization of the property evolution with time.

torsions may vary but not necessary towards the t–g–g–t conformation. This implies that the torsion forces may be compromised by the vdW forces as the cluster develops. It is also interesting to note that, at low temperatures (e.g. 350 K), the backbone torsions may be trapped in poor conformations as the segments have less kinetic energy to overcome the torsion barrier. However, at higher temperatures (400 and 450 K) we often observe the increase of the t–g–g–t fraction as the segments have sufficient energy to overcome torsion barriers should it ever enter the non t–g–g–t conformation due to vdW forces. In other words, with sufficient energy to overcome the torsional barriers, the conformation of the O–CH_2–CH_2–CH_2–O preferentially evolves towards the trans–gauche–gauche–trans (t–g–g–t) conformation [70, 71], which is favored for the formation of a more compact nucleus.

3.5. Results from larger-sized systems

The larger systems (containing eight polymer chains, each with a degree of polymerization of 27) were prepared from scratch (not by duplicating any of the samples used previously) and then equilibrated following the same procedure described in this paper. The time variation of the cluster fraction and the temperature dependence of the average cluster fraction are shown in figure 9 and the size and number of ordered clusters

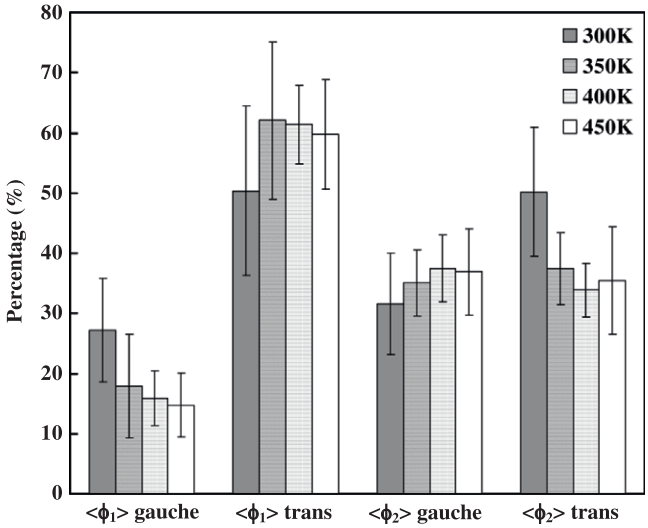

Figure 8. The distribution of backbone torsions ϕ_1 and ϕ_2 in the gauche or trans states at 300, 350, 400 and 450 K.

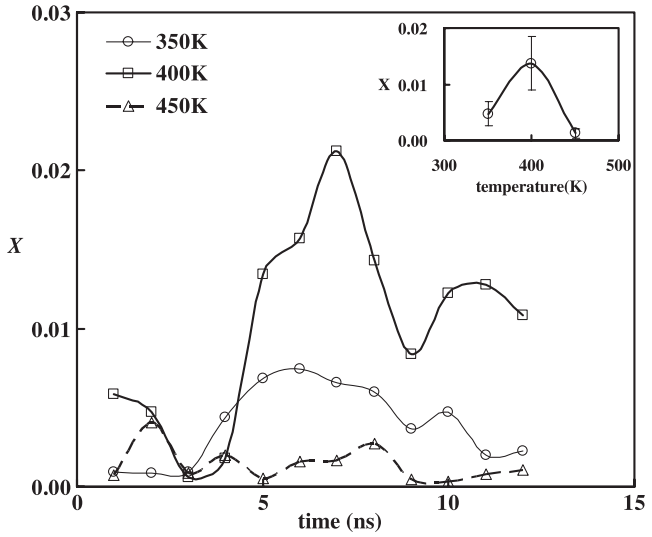

Figure 9. The variation of the number of clusters (defined in equation (2)) with time at 350, 400 and 450 K using a double-sized (216-segment) system. The inset shows the variation of the average number of clusters (defined in equation (2)) with temperature.

are summarized in table 3. While the distribution of clusters and absolute values of X are not the same as that obtained from the small-sized samples (which is an indication of the effect of local chain packing on the cluster formation), the behaviors (variation local ordering with time and the occurrence of maximum local ordering at temperature 400 K) are the same as those observed previously. Since the initial structure formation is highly dependent on the initial condition and the two sets of simulations are completely independent, some difference in the absolute value of X is expected. Considering that the simulation time is shorter for the larger system, the number of segments contained in the largest ordered structures are similar from the two sets of simulations, and the fluctuation in the size of order structures, we believe that such differences are reasonable. We find that the initial structural development of PTT is dominated by local segment fluctuations. Such local fluctuations are ubiquitous and do not decay with the increase of system size. We thus believe that the mechanism of the initial formation of ordered clusters and the temperature effects observed here are not affected by the system size used in our simulation.

3.6. Possible mechanism of crystallization

Based on the simulation results, we propose that the orientationally ordered clusters may be the baby nuclei [5, 21] that are suggested to form in the early stage of the crystallization process. Such baby nuclei have a high internal orientation order but are loosely packed. The baby nuclei are constantly forming, growing and disintegrating. Their formation is mainly driven by van der Waals and torsional forces. These two forces may either collaborate or compete, resulting in the segment to reorganize to form a more compact cluster. Therefore, the baby nuclei could eventually become compact nuclei along the crystallization process. However, internal structural development of such baby nuclei (e.g. torsional reorganization) takes place at a much slower rate (compared to the formation of baby nuclei). As a consequence, there is observed (experimentally) a long induction period prior to the crystallization of polymers.

It should be noted that, while the formation of orientationally ordered clusters is clearly observed in PTT, we do not rule out the possibility that the mechanism of the formation and development of such baby nuclei may be different for a polymer with a different molecular structure. The π/π interactions between the aromatic rings of PTT may help the formation of ordered segment clusters. For polymers without orientationally independent intersegmental interactions, e.g. polyethylene, the nucleation/crystallization may follow a mechanism different from the one suggested here.

4. Conclusions

The formation of local structural ordering in the early stage of crystallization of polymer PTT from melt is observed in our simulation. The thermal properties such as T_g and T_m of the PTT are accurately predicted. Between these temperatures, the torsional and van der Waals forces drive the segments to form clusters consisting of parallel segments. The number of such orientationally ordered clusters increases rapidly soon after the system is cooled and then fluctuates around some asymptotic value. During this later stage, it is found that the torsional distribution of the polymer backbone for segments within the cluster slowly rearranges to that in the crystalline state. In addition, the temperature variation of the number of clusters resembles that of the crystallization rate between T_g and T_m. The formation and development of these clusters follows the growth–nucleation mechanism. It is likely that the clusters are the baby nuclei suggested by other researchers in the early stage of the crystallization process.

Acknowledgments

We would like to thank the financial support from grant NSC 95-2221-E-002-290 by the National Science Council of Taiwan and computation resources from the National Center for High-Performance Computing of Taiwan.

References

[1] Huang J M and Chang F C 2000 *J. Polym. Sci.* B **38** 934–41
[2] Wang X S, Yan D Y, Tian G H and Li X G 2001 *Polym. Eng. Sci.* **41** 1655–64
[3] Hong P D, Chuang W T, Yeh W J and Lin T L 2002 *Polymer* **43** 6879–86
[4] Xu Y, Ye S R, Bian J and Qian J W 2004 *J. Mater. Sci.* **39** 5551–5
[5] Muthukumar M 2000 *Eur. Phys. J.* E **3** 199–202
[6] Yamamoto T 2005 *Interphases Mesophases in Polymer Crystallization III* vol 191 (Berlin: Springer) pp 37–85
[7] Olmsted P D, Poon W C K, McLeish T C B, Terrill N J and Ryan A J 1998 *Phys. Rev. Lett.* **81** 373–6
[8] Yamamoto T 2001 *J. Chem. Phys.* **115** 8675–80
[9] ten Wolde P R and Frenkel D 1999 *Phys. Chem. Chem. Phys* **1** 2191–6
[10] Akpalu Y, Kielhorn L, Hsiao B S, Stein R S, Russell T P, van Egmond J and Muthukumar M 1999 *Macromolecules* **32** 765–70
[11] Terrill N J, Fairclough P A, Towns-Andrews E, Komanschek B U, Young R J and Ryan A J 1998 *Polymer* **39** 2381–5
[12] Ezquerra T A, Sanchez-Cuesta M, Ungar G, Feijoo J L and Lopez-Cabarcos E 1998 *J. Polym. Sci.* B **36** 49–54
[13] Imai M, Kaji K, Kanaya T and Sakai Y 1995 *Phys. Rev.* B **52** 12696–704
[14] Heeley E L, Maidens A V, Olmsted P D, Bras W, Dolbnya I P, Fairclough J P A, Terrill N J and Ryan A J 2003 *Macromolecules* **36** 3656–65
[15] Strobl G 2006 *Prog. Polym. Sci.* **31** 398–442
[16] Fukao K and Miyamoto Y 1997 *Phys. Rev. Lett.* **79** 4613–6
[17] Soccio M, Nogales A, Lotti N, Munari A and Ezquerra T A 2007 *Phys. Rev. Lett.* **98** 037801
[18] Rieger J 2003 G Reiter, J U Sommer (eds) *Polymer Crystallization: Observations, Concepts, and Interpretations* (Berlin: Springer) pp 9–16
[19] Strobl G 2000 *Eur. Phys. J.* E **3** 165–83
[20] Sasaki S, Tashiro K, Kobayashi M, Izumi Y and Kobayashi K 1999 *Polymer* **40** 7125–35
[21] Panine P, Urban V, Boesecke P and Narayanan T 2003 *J. Appl. Crystall.* **36** 991–4
[22] Wang Z G, Hsiao B S, Sirota E B, Agarwal P and Srinivas S 2000 *Macromolecules* **33** 978–89
[23] Panine P, Di Cola E, Sztucki A and Narayanan T 2008 *Polymer* **49** 676–80
[24] Ko M J, Waheed N, Lavine M S and Rutledge G C 2004 *J. Chem. Phys.* **121** 2823–32
[25] Hu W B 2005 *Macromolecules* **38** 8712–8
[26] Wang M X, Hu W B, Ma Y and Ma Y Q 2005 *Macromolecules* **38** 2806–12
[27] Lavine M S, Waheed N and Rutledge G C 2003 *Polymer* **44** 1771–9
[28] Yashiro K, Ito T and Tomita Y 2003 *Int. J. Mech. Sci.* **45** 1863–76
[29] Koyama A, Yamamoto T, Fukao K and Miyamoto Y 2002 *Phys. Rev.* E **65** 050801
[30] Dukovski I and Muthukumar M 2003 *J. Chem. Phys.* **118** 6648–55
[31] Yamamoto T 2004 *Polymer* **45** 1357–64
[32] Gee R H, Lacevic N and Fried L E 2006 *Nat. Mater.* **5** 39–43
[33] Koyama A, Yamamoto T, Fukao K and Miyamoto Y 2001 *J. Chem. Phys.* **115** 560–6
[34] Takeuchi H 1998 *J. Chem. Phys.* **109** 5614–21
[35] Iwata M and Sato H 1999 *Phys. Chem. Chem. Phys.* **1** 2491–500
[36] Meyer H and Muller-Plathe F 2002 *Macromolecules* **35** 1241–52
[37] Liu C and Muthukumar M 1998 *J. Chem. Phys.* **109** 2536–42
[38] Muthukumar M and Welch P 2000 *Polymer* **41** 8833–7
[39] Malvaldi M, Allegra G, Ciardelli F and Raos G 2005 *J. Phys. Chem.* B **109** 18117–26
[40] Miura T and Mikami M 2007 *Phys. Rev.* E **75** 031804
[41] Zhang J L 2004 *J. Appl. Polym. Sci.* **91** 1657–66
[42] Yang J S and Jo W H 2001 *J. Chem. Phys.* **114** 8159–64
[43] Wu J, Schultz J M, Samon J M, Pangelinan A B and Chuah H H 2001 *Polymer* **42** 7141–51
[44] Wu J and Schultz J M 2002 *Polymer* **43** 6695–700
[45] Srimoaon P, Dangseeyun N and Supaphol P 2004 *Eur. Polym. J.* **40** 599–608
[46] Park S C, Liang Y R, Lee H S and Kim Y H 2004 *Polymer* **45** 8981–8
[47] Ohtaki M, Kameda T, Asakura T and Murase S 2005 *Polym. J.* **37** 214–20
[48] Jeong Y G, Bae W J and Jo W H 2005 *Polymer* **46** 8297–305
[49] Jang S S and Jo W H 1999 *J. Chem. Phys.* **110** 7524–32
[50] Hong P D, Chung W T and Hsu C F 2002 *Polymer* **43** 3335–43
[51] He X J, Chuah H H and Ellison M S 2004 *Polym. Bull.* **51** 285–91
[52] Frisk S, Ikeda R M, Chase D B, Kennedy A and Rabolt J F 2004 *Macromolecules* **37** 6027–36
[53] Chung W T, Yeh W J and Hong P D 2002 *J. Appl. Polym. Sci.* **83** 2426–33
[54] Chuah H H 2001 *Macromolecules* **34** 6985–93
[55] Ward I M, Wilding M A and Brody H 1976 *J. Polym. Sci.* B **14** 263–74
[56] Allegra G and Meille S V 1999 *Phys. Chem. Chem. Phys.* **1** 5179–88
[57] Cerius^2 2003 (San Diego: Accelrys Inc.)
[58] Mark J E 1996 *Physical Properties of Polymers Handbook* (New York: AIP Press)
[59] Plimpton S 1995 *J. Comput. Phys.* **117** 1–19
[60] Darden T, York D and Pedersen L 1993 *J. Chem. Phys.* **98** 10089–92
[61] Plimpton S J, Pollock R and Stevens M 1997 Particle-mesh ewald and rRESPA for parallel molecular dynamics simulations *Proc. 8th SIAM Conf. on Parallel Processing for Scientific Computing (Minneapolis, MN)*
[62] Hoover W G 1985 *Phys. Rev.* A **31** 1695–7
[63] Nose S 1984 *Mol. Phys.* **52** 255–68
[64] Mayo S L, Olafson B D and Goddard W A 1990 *J. Phys. Chem.* **94** 8897–909
[65] Becke A D 1993 *J. Chem. Phys.* **98** 5648–52
[66] Lee C T, Yang W T and Parr R G 1988 *Phys. Rev.* B **37** 785–9
[67] Miehlich B, Savin A, Stoll H and Preuss H 1989 *Chem. Phys. Lett.* **157** 200–6
[68] Johnson B G, Gill P M W and Pople J A 1993 *J. Chem. Phys.* **98** 5612–26
[69] Frisch M J, Trucks G W, Schlegel H B, Scuseria G E, Robb M A, Cheeseman J R, Zakrzewski V G, Montgomery J A, Stratmann J R E, Burant J C, Dapprich S, Millam J M, Daniels A D, Kudin K N, Strain M C, Farkas O, Tomasi J, Barone V, Cossi M, Cammi R, Mennucci B, Pomelli C, Adamo C, Clifford S, Ochterski J, Petersson G A, Ayala P Y, Cui Q, Morokuma K, Malick D K, Rabuck A D,

Raghavachari K, Foresman J B, Cioslowski J, Ortiz J V, Stefanov B B, Liu G, Liashenko A, Piskorz P, Komaromi I, Gomperts R, Martin R L, Fox D J, Keith T, Al-Laham M A, Peng C Y, Nanayakkara A, Gonzalez C, Challacombe M, Gill P M W, Johnson B, Chen W, Wong M W, Andres J L, Gonzalez C, Head-Gordon M, Replogle E S and Pople J A 1998 *Gaussian 98* (Pittsburgh, PA: Gaussian)

[70] Desborough I J, Hall I H and Neisser J Z 1979 *Polymer* **20** 545–52

[71] Poulindandurand S, Perez S, Revol J F and Brisse F 1979 *Polymer* **20** 419–26

[72] Jakeways R, Ward I M, Wilding M A, Hall I H, Desborough I J and Pass M G 1975 *J. Polym. Sci.* B **13** 799–813

[73] Hsieh M-K 2008 Early state crystallization process of poly (trimethylene terephthalate) (PTT) polymer from atomistic molecular dynamics simulations *Master Thesis* National Taiwan University

[74] Capaldi F M, Boyce M C and Rutledge G C 2004 *Polymer* **45** 1391–9

[75] Sperling L H 2006 *Introduction to Physical Polymer Science* (Hoboken, NJ: Wiley)